

Pietra-Ricci Index Detector for Centralized Data Fusion Cooperative Spectrum Sensing

Dayan Adionel Guimarães

Abstract—The Pietra-Ricci index is often used in economic and social sciences as a measure of inequality. In this Correspondence, the index is adapted to the cooperative spectrum sensing scenario, yielding the Pietra-Ricci index detector (PRiDe). The PRiDe applies the index to distinguish the shapes of the received signal sample covariance matrices in the situations of presence and absence of the primary sensed signal. It is shown that the PRiDe is very simple, is robust against time-varying noise and received signal powers, exhibits the constant false alarm rate property, and outperforms state-of-the-art detectors in many situations.

Index Terms—Cognitive radio, Gini index, cooperative spectrum sensing, Pietra-Ricci index.

I. INTRODUCTION

THE radio-frequency (RF) spectrum is currently crowded due to the large amount of wireless communication systems in operation, and due to the adoption of a fixed allocation policy in which a primary user (PU) network is granted exclusive use of a given RF band. The situation tends to worsen with the massive deployment of the Internet of Things (IoT) and the fifth generation (5G) of wireless communication networks, mainly due to the expected large number of terminals and the demand for higher bandwidths.

The cognitive radio (CR) concept has emerged as a potential solution to the RF spectrum shortage [1], [2], exploring the varying nature of the spectrum occupation in time and space. A CR network can adopt a dynamic spectrum access policy in which unoccupied frequency bands can be opportunistically used by cognitive secondary user (SU) terminals. In order to detect the presence of the PU signals in the band of interest, the SUs apply a process called spectrum sensing [2], [3], possibly assisted by an RF spectrum occupancy database [4].

Spectrum sensing can be made independently by each SU, or can resort to cooperation. The former is subjected to problems that reduce the PU signal detection power, like multipath fading, shadowing and hidden terminals [2]. Cooperation improves the accuracy of the decisions on the spectrum occupation, thanks to the spatial diversity promoted by the different locations of the SUs in cooperation.

In centralized cooperative spectrum sensing (CSS) with data fusion, which is considered herein, samples of the received

signal, or quantities derived therefrom, are transmitted to a fusion center (FC) where a test statistic is formed and the global decision is made. This decision is informed to the SUs, which will compete for the band if it is vacant, by means of some multiple access protocol.

A. Related research

Many of the test statistics developed so far for spectrum sensing are formed by processing the received signal sample covariance matrix (SCM). This processing often involves matrix computations like the determinant, the trace, as well as eigenvalues and eigenvectors. Examples of detectors that process the SCM are the Hadamard ratio (HR) detector [5], [6], the arithmetic to geometric mean (AGM) detector [7], the volume-based detectors (VD) [8], [9], the maximum-minimum eigenvalue detector (MMED), the eigenvalue-based generalized likelihood ratio test (GLRT) [10], and the Gini index detector (GID) [11]. These detectors are blind in the sense that they do not demand the knowledge of the noise variance, neither the characteristics of the signal to be detected.

Among the above detectors, the GID deserves especial attention for exhibiting computational complexity much smaller than the other ones, robustness against variations in the received signal and noise powers, and high detection power when the signal has a dominant propagation path component, either line-of-sight or specular.

B. Contribution and structure of the paper

This Correspondence proposes the Pietra-Ricci index detector (PRiDe) for centralized data fusion CSS. The PRiDe test statistic is easily computed from the elements of the received signal SCM, which makes it much less complex than the detectors HR, AGM, VD, MMED, and the eigenvalue-based GLRT, and even a little less complex than the GID. In fact, to the best of the authors knowledge, the PRiDe is the less complex blind detector available so far. It is also robust against nonuniform and time-varying received signal and noise levels, attains the constant false alarm rate (CFAR) property, and outperforms the above detectors in several circumstances.

The remainder of the article is organized as follows. Section II describes the system model. The PRiDe is proposed in Section III. Numerical results and analyses are given in Section IV. The main conclusions are drawn in Section V.

II. SYSTEM MODEL

The centralized CSS with data fusion is accomplished by m cognitive SUs, each one collecting n samples of the signal

Copyright (c) 2020 IEEE. Personal use of this material is permitted. However, permission to use this material for any other purposes must be obtained from the IEEE by sending a request to pubs-permissions@ieee.org.

Dayan A. Guimarães is with the National Institute of Telecommunications (Inatel), PO Box 05, 37540-000, Santa Rita do Sapucaí, MG, Brazil (Tel: +55 35 3471 9227, Fax: +55 35 3471 9314, e-mail: dayan@inatel.br).

This work was supported in part by CNPq, Grant 308365/2017-8, and RNP, with resources from MCTIC, Grant 01250.075413/2018-04, under the Radiocommunication Reference Center (CRR) project of Inatel.

received from a single PU transmitter during each sensing interval. At the FC, these samples form the matrix $\mathbf{Y} \in \mathbb{C}^{m \times n}$ given by

$$\mathbf{Y} = \mathbf{h}\mathbf{x}^T + \mathbf{V}. \quad (1)$$

In this equation, the samples associated to the signal transmitted by the PU form the vector $\mathbf{x} \in \mathbb{C}^{n \times 1}$. These samples are zero-mean complex Gaussian random variables whose variance is set according to the average signal-to-noise ratio (SNR) across the SUs. The Gaussian distribution is adopted due to the fact that it appropriately describes the envelope fluctuations of typical modulated and filtered digital communication signals [10].

The channel vector $\mathbf{h} \in \mathbb{C}^{m \times 1}$ in (1) has elements h_i , $i = 1, 2, \dots, m$, representing the flat channel gains between the PU and the i -th SU. These gains are constant during the sensing interval and independent and identically distributed (i.i.d.) between consecutive sensing rounds. The channel vector is given by $\mathbf{h} = \mathbf{G}\mathbf{a}$, where \mathbf{G} is a gain matrix to be defined later, and the vector $\mathbf{a} \in \mathbb{C}^{m \times 1}$ has elements $a_i \sim \mathcal{CN}[\sqrt{\kappa_i}/(2\kappa_i + 2), 1/(\kappa_i + 1)]$, yielding $\mathbb{E}\{|a_i|^2\} = 1$, with κ_i being the Rice factor¹ of the channel between the PU and the i -th SU. To model extremes of realistic scenarios, $\kappa_i = 10^{K_i/10}$, where $K_i \sim \mathcal{N}[\mu_K, \sigma_K]$, with $\mu_K = 1.88$ dB and $\sigma_K = 4.13$ dB for urban areas, and $\mu_K = 2.63$ dB and $\sigma_K = 3.82$ dB for rural and open areas [12].

In practice, the SNR across the SUs is time-varying and dependent of the SUs' locations. This is owed to the main reasons: i) time-varying received signal levels are produced by different distance-dependent path losses between the PU and the potentially moving SUs, and ii) receiver calibration errors, as well as changes in low noise amplifier (LNA) gains and environmental temperature cause variations in the thermal noise level generated in the receiver circuitry.

Different (i.e., nonuniform) received signal levels across the SUs may be considered in the present model by setting the gain matrix $\mathbf{G} \in \mathbb{R}^{m \times m}$ as $\mathbf{G} = \text{diag}(\sqrt{\mathbf{p}/p_{\text{avg}}})$, where the vector $\mathbf{p} = [p_1, p_2, \dots, p_m]$ contains the received signal powers across the SUs, and $p_{\text{avg}} = (1/m) \sum_{i=1}^m p_i$ is the average received signal power over all SUs. Since the average channel power gain is unitary, without loss of generality, the PU transmits with a constant power p_{avg} . If nonuniform and time-varying received signal powers are assumed, then $p_i \sim \mathcal{U}[(1 - \rho)p_{\text{avg}}, (1 + \rho)p_{\text{avg}}]$ in each sensing round, where ρ is the fractional variation about the average. In the case of nonuniform and time-varying noise, the elements in the i -th row of the matrix $\mathbf{V} \in \mathbb{C}^{m \times n}$ in (1) are i.i.d. Gaussian noise samples with zero mean and variance $\sigma_i^2 \sim \mathcal{U}[(1 - \rho/2)\sigma_{\text{avg}}^2, (1 + \rho/2)\sigma_{\text{avg}}^2]$ in each sensing round, where $\sigma_{\text{avg}}^2 = (1/m) \sum_{i=1}^m \sigma_i^2$ is the average noise variance across the SUs. Thus, the fraction of noise power variation is arbitrarily set as half the fraction of signal power variation. The received SNR, in dB, averaged over all SUs, is $\text{SNR} = 10 \log_{10}(p_{\text{avg}}/\sigma_{\text{avg}}^2)$.

¹In a multipath fading channel, the Rice factor is the ratio between the power in the dominant multipath component and the power of the remaining ones. If $\kappa_i = 0$, the Ricean fading specializes to the Rayleigh fading. If $\kappa_i \rightarrow \infty$, a pure additive white Gaussian noise (AWGN) channel results. For practical purposes, an almost-pure AWGN channel is observed if $\kappa_i > 10$.

It is worth noting that the CSS with multiple SUs in cooperation is equivalent to the spectrum sensing made by a single SU with multiple antennas, in terms of the model given in (1). However, the channel vector \mathbf{h} preferably must take into account the particularities of a CSS with single-antenna SUs or a single SU with multiple antennas. Here, the channel model has been chosen to fit the CSS scenario.

Given \mathbf{Y} at the FC, the SCM of order m is computed as

$$\mathbf{R} = \frac{1}{n} \mathbf{Y} \mathbf{Y}^\dagger, \quad (2)$$

where \dagger denotes the complex conjugate and transpose operation. Under the hypothesis \mathcal{H}_0 , the primary signal is absent in the band of interest, that is $\mathbf{Y} = \mathbf{V}$. Under the hypothesis \mathcal{H}_1 , the primary signal is present, that is, $\mathbf{Y} = \mathbf{h}\mathbf{x}^T + \mathbf{V}$.

The metrics often used to assess the spectrum sensing performance are the probability of detection, P_d , and the probability of false alarm, P_{fa} . The former is the probability of deciding in favor of an occupied band, given that it is really occupied. The latter is the probability of deciding in favor of an occupied band, given that it is in fact vacant.

III. THE PIETRA-RICCI INDEX DETECTOR

When the signal detection theory is applied to the spectrum sensing binary hypothesis test problem, it quite often yields elegant developments of detectors, but in most cases the assumptions made to allow for a mathematically tractable solution do not guarantee satisfactory operation in all scenarios of practical interest. Here, instead of applying such theory, the detector is devised based on an existing statistical metric, specifically an index used in economic and social sciences as a measure of inequalities, which is the Pietra-Ricci index [13], also known as Hoover index, Robin Hood index or Schutz index. The Pietra-Ricci index is given by

$$P = \frac{\sum_i |x_i - \bar{x}|}{2 \sum_i x_i}, \quad (3)$$

where $|\cdot|$ denotes the absolute value operation, x_i is the income of the i -th person and \bar{x} is the mean income. The index P measures the portion of income that would be taken from the privileged (richer) half of the population in analysis and given to the less privileged (poorer) half in order to achieve equality.

To adapt the Pietra-Ricci index to the spectrum sensing scenario, the incomes operated in (3) need to be translated into a quantity obtained from the spectrum sensing process. Here, the index is used to measure the inequality level between the received signal SCM elements when the PU signal state changes. To illustrate this concept, Fig. 1 depicts the mesh surface plot of the absolute values of the elements of an SCM under the hypotheses of absence (left) and presence (right) of the PU signal. If these values are viewed as incomes, the Pietra-Ricci index can be used to distinguish the SCMs and, thus, can be applied as a binary hypothesis test statistic for spectrum sensing. A similar reasoning has been followed in [11] to adapt the Gini index to the binary hypothesis test associated to the spectrum sensing problem.

Let r_i denote the i -th element of the vector formed by stacking all columns of \mathbf{R} , and let $\bar{r} = (1/m^2) \sum_i r_i$. The Pietra-Ricci index detector (PRIDE) test statistic is defined as

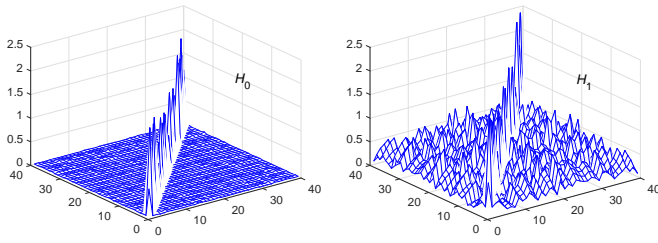


Fig. 1. Mesh surface plot of an SCM under \mathcal{H}_0 (left) and \mathcal{H}_1 (right), for $m = 40$, $n = 10000$, $\text{SNR} = -5$ dB, and $\kappa_i = 10$ for $i = 1, \dots, 40$.

$$T_{\text{PRIDe}} = \frac{\sum_{i=1}^{m^2} |r_i|}{\sum_{i=1}^{m^2} |r_i - \bar{r}|}. \quad (4)$$

The factor 2 in (3) is not being used in (4), since it does not affect performance. The reciprocal of (3) has been adopted in (4) for convenience, such that, given a decision threshold γ , if $T_{\text{PRIDe}} > \gamma$ the decision is made in favor of \mathcal{H}_1 ; otherwise the decision is in favor of \mathcal{H}_0 . Additionally, the absolute value of r_i is used in (4) since this quantity can be complex.

Clearly, the computation of (4) is quite simple, which is a desirable attribute. Moreover, (4) is formed by a ratio of two quantities that, by construction, are affected in the same proportion by the noise variance, conferring the CFAR property to the PRIDe. This property allows for the configuration of γ to yield a target P_{fa} , independent of the noise variance. To demonstrate this property, Fig. 2 shows empirical probability density functions (PDFs) obtained from 50000 values of (4) under \mathcal{H}_0 and \mathcal{H}_1 , for $\sigma_{\text{avg}}^2 = 1$ (left) and $\sigma_{\text{avg}}^2 = 10$ (right), $m = 5$ SUs, $n = 150$ samples per SU, $\rho = 0.95$, and a rural area. The PU transmit power was set to keep the SNR fixed in -12 dB for both values of σ_{avg}^2 . It can be seen that the PDFs under \mathcal{H}_0 are identical in shape and support, meaning that the area on the right of any γ , which corresponds to P_{fa} , will be the same no matter the value of σ_{avg}^2 . Hence, the PRIDe detector indeed attains the CFAR property.

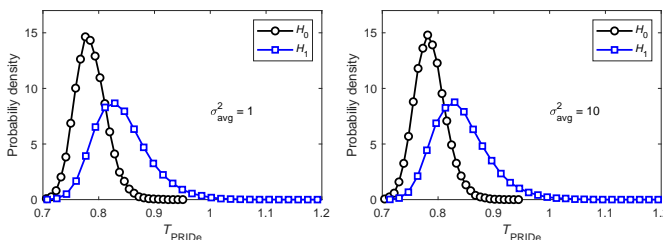


Fig. 2. Empirical PDFs of (4) for $\sigma_{\text{avg}}^2 = 1$ (left) and $\sigma_{\text{avg}}^2 = 10$ (right), with $m = 5$, $n = 150$, $\rho = 0.95$, rural area and $\text{SNR} = -12$ dB.

IV. COMPARATIVE ANALYSES

In this section, the PRIDe is compared with the detectors GID, HR, AGM, VD number 1 (VD1), MMED, and GLRT, in terms of complexity and performance, the latter obtained by computer simulations using the MATLAB software. The competing test statistics are given in Table I, where $\lambda_1 \geq \lambda_2 \geq \dots \geq \lambda_m$ are the eigenvalues of \mathbf{R} , $\det(\mathbf{R})$

is the determinant of \mathbf{R} , r_{ij} is the element in the i -th row and j -th column of \mathbf{R} , and $\mathbf{E} = \text{diag}(\mathbf{d})$, where $\text{diag}(\mathbf{d})$ is the diagonal matrix whose main diagonal forms the vector $\mathbf{d} = [d_1, d_2, \dots, d_m]$, with $d_i = \|\mathbf{R}(i, :)\|_2$, being $\|\cdot\|_2$ the Euclidean norm.

TABLE I
COMPETING TEST STATISTICS

$T_{\text{GID}} = \frac{\sum_{i=1}^{m^2} r_i }{\sum_{i=1}^{m^2} \sum_{j=1}^{m^2} r_i - r_j }$	$T_{\text{AGM}} = \frac{\frac{1}{m} \sum_{i=1}^m \lambda_i}{\left(\prod_{i=1}^m \lambda_i\right)^{1/m}}$
$T_{\text{HR}} = \frac{\det(\mathbf{R})}{\prod_{i=1}^m r_{ii}}$	$T_{\text{GLRT}} = \frac{\lambda_1}{\sum_{i=1}^m \lambda_i}$
$T_{\text{VD1}} = \log [\det(\mathbf{E}^{-1} \mathbf{R})]$	$T_{\text{MMED}} = \frac{\lambda_1}{\lambda_m}$

A. Computational complexity

The computational complexity of the GID is dominated by the cost of calculating the SCM, which is $O(nm^2)$ [14]. The other test statistics shown in Table I have similar complexities, around $O(nm^2)$ for computing the SCM, plus the complexity related to calculating eigenvalues and determinants, which costs around $O(m^3)$ [11], [14]. Hence, the complexities of computing T_{PRIDe} and T_{GID} are similar and by far smaller than the other ones. In detail, the complexity of the PRIDe is even smaller than the complexity of the GID, since the former executes $m^2 - 1$ times less additions than the latter in the denominator of the test statistic.

B. Simulated performance results

The performance results shown hereafter give P_d as a function of the most relevant system parameters, for a constant $P_{\text{fa}} = 0.1$ [4]. Each point on all curves was determined from 50000 Monte Carlo computer simulation runs, corresponding to the generation of the same number of each test statistic under \mathcal{H}_0 and \mathcal{H}_1 , for the same amount of transmitted signal, noise and channel realizations. The MATLAB simulation code is available at [15]. The average SNR or the number of samples n was adjusted in some cases to guarantee that the P_d attained by the best detector became close to 0.9, which is a reference target in the IEEE 802.22 standard [4], around the mid-value of the parameter varied, so that values of P_d below and above this reference may be seen throughout the whole best result.

Fig. 3 gives P_d versus the fraction ρ that governs the noise and signal power variations, for an urban area and $\text{SNR} = -10$ dB (left), and for a rural area and $\text{SNR} = -10.4$ dB (right). It is clear that the detectors PRIDe, GID, HR and VD1 are very robust against these variations. The GLRT, the MMED and the AGM are not robust at all. Moreover, it can be seen that the PRIDe is considerably superior to the GID and a little superior to the HR and the VD1 for any ρ . Recall that the GID is the only detector whose complexity approximates the complexity of the PRIDe; the other ones are much more complex.

Hereafter, only nonuniform and time-varying noise and signal powers with $\rho = 0.95$ are assumed, since uniform and fixed levels for these quantities are unrealistic.

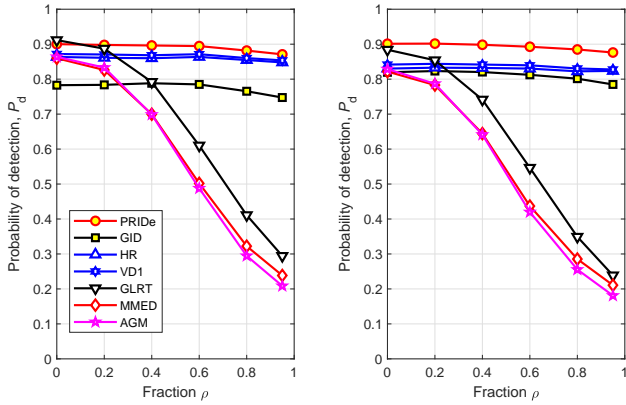


Fig. 3. P_d versus ρ for $m = 5$, $n = 200$, and $P_{fa} = 0.1$: urban area and SNR = -10 dB (left); rural area and SNR = -10.4 dB (right).

4

Fig. 3 shows results of P_d versus the average SNR across the SUs, for an urban area and $n = 200$ (left), and for a rural area and $n = 160$ (right). The PRIDe achieves comparable or the best performance for any SNR, outperforming the GID in most of the analyzed SNRs. The detectors GLRT, MMED and AGM unveiled poor performances due to their non robustness to signal and noise power variations, except at very high SNRs.

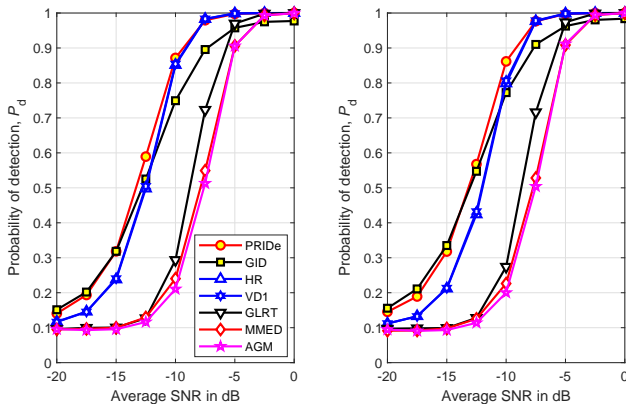


Fig. 4. P_d versus SNR for $m = 5$, $\rho = 0.95$, and $P_{fa} = 0.1$: urban area and $n = 200$ (left); rural area and $n = 160$ (right).

Fig. 5 gives P_d versus the number of samples n , for an urban area and SNR = -11.5 dB (left), and for a rural area and SNR = -12 dB (right). The influence of the number of SUs m on P_d is depicted in Fig. 6 for an urban area and SNR = -11 dB (left), and for a rural area and SNR = -11.5 dB (right). From these figures it can be seen that the PRIDe is capable of outperforming the other detectors for any n and m . The GLRT, MMED and AGM are useless in the setup of Fig. 5, yielding poor performances in the case of Fig. 6, owed to their poor robustness against signal and noise power variations.

In general, it can be noticed in Figs. 3-6 that the performances of the GID and the PRIDe have become closer to each other when the environment changed from urban to rural. This is owed to the facts that rural areas are subjected to larger Rice factors than urban areas, on average, and that the GID achieves very good performances when the Rice factor is large [11].

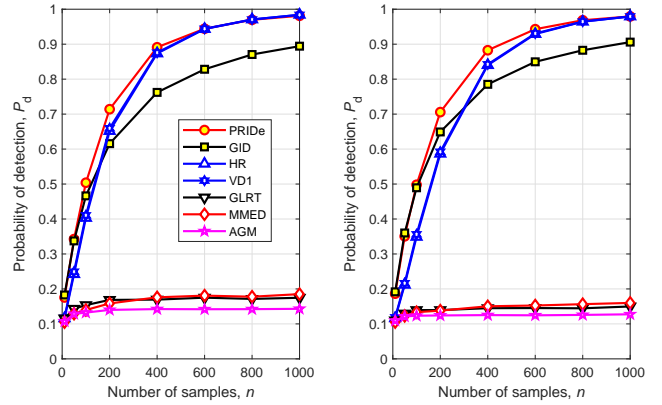


Fig. 5. P_d versus n for $m = 5$, $\rho = 0.95$, and $P_{fa} = 0.1$: urban area and SNR = -11.5 dB (left); rural area and SNR = -12 dB (right).

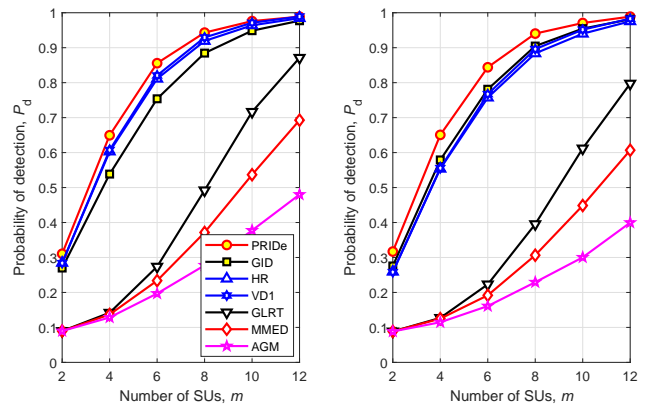


Fig. 6. P_d versus m for $n = 200$, $\rho = 0.95$, and $P_{fa} = 0.1$: urban area and SNR = -11 dB (left); rural area and SNR = -11.5 dB (right).

Interesting enough, the gaps between the performances of the PRIDe and the other detectors analyzed have increased when the environment changed from urban to rural.

C. Theoretical performance considerations and SNR walls

Up to the moment of preparation of this Correspondence, the expressions for the PDFs or the cumulative distribution functions (CDFs) of T_{PRIDe} under \mathcal{H}_0 , respectively $f(t|\mathcal{H}_0)$ and $F(t|\mathcal{H}_0)$, and under \mathcal{H}_1 , respectively $f(t|\mathcal{H}_1)$ and $F(t|\mathcal{H}_1)$, are unknown. These expressions are hard or intractable to derive analytically, thus preventing the theoretical computation of P_d , P_{fa} and γ .

In order to circumvent the problem of unknown theoretical distributions, one may resort to a semi-analytical approach in which they are found via a goodness-of-fit method, with distribution parameters obtained through an appropriate method for mapping them into the CSS parameters, for instance using simple artificial neural networks. Such approach has been successfully applied in [16] in the case of the GID detector, and can be adapted to the PRIDe with minor effort.

Another performance metric is the SNR wall, which is the SNR value below which it is not possible to achieve an unlimited reliability in terms of P_d and P_{fa} , no matter the number of collected samples, n [17]. This classical definition applies to

detectors that make use of the noise variance information, thus being dependent of the uncertainty on this information. In [18], the SNR wall is alternatively defined as the SNR value below which the medians of the test statistic distributions under the two hypotheses overlap, for a sufficiently large n , which means that either P_{fa} or $1 - P_d$ becomes larger than 0.5. This definition is applicable to all test statistics in analysis herein, since they do not make use of the noise variance, as already demonstrated in [18] for the MMED. Moreover, the SNR wall defined in this way is relatively easy to compute, yielding results that closely approximate known theoretical ones [18].

The SNR walls associated with the detectors considered in this Correspondence are shown in Table II, for urban and rural environments, assuming $m = 5$, $n = 10000$, $\rho = 0.95$, and 50000 values of each test statistic, for each hypothesis. For each detector, the average SNR was decremented in steps of 0.5 dB, departing from a value surely above the SNR wall, until the median of the test statistic associated to \mathcal{H}_1 crossed the median associated to \mathcal{H}_0 . The SNR at this point was recorded as the SNR wall.

TABLE II
EMPIRICAL SNR WALLS, IN DECIBELS

	PRIDe	GID	AGM	HR	GLRT	VDI	MMED
Urban	-38.5	-40.5	-15.5	-36.0	-18.5	-32.0	-17.0
Rural	-40.0	-42.0	-15.5	-34.0	-18.5	-31.5	-17.0

Table II demonstrates that SNR walls exist even when the detector does not use the noise variance information, as also noted in [18]. The table also unveils results in agreement with those in Figs. 3–6 for all detectors, that is, an increase (resp. decrease) in the SNR wall from the urban to the rural environment is consistent with a performance degradation (resp. improvement). When checking this behavior, one must be aware of changes in the number of samples, n , or in the average SNR, from one environment to the other. Notice also that the SNR walls of the GID are smaller than in the case of the PRIDe, meaning that the former is capable of outperforming the latter in very small SNR regimes, as can be confirmed from Fig. 4. Moreover, the performance ranking observed in Figs. 3–6 closely matches the ordering of the SNR walls, except in the case of the PRIDe and the GID due to the low SRN regime, as already explained. The close proximity of the results attained by the HR and the VDI detectors in Fig. 4 at low SNRs prevent accurate comparisons in this regard.

V. CONCLUSIONS

This Correspondence proposed the Pietra-Ricci index detector (PRIDe) for centralized cooperative spectrum sensing with data fusion. The computational complexity of the PRIDe test statistic is the smallest among all blind detectors identified in the literature. Moreover, the PRIDe is robust against time-varying nonuniform received signal and noise powers, attains the constant false alarm rate property, and outperforms state-of-the-art detectors in many circumstances. The reported simulation results were supported by an empirical SNR wall analysis, and by a system model that takes into account typical sensing channel characteristics found in the

real world, namely: the combination of fading and thermal noise, the variation of received signal and noise powers across the spectrum sensors, and the dynamics of the line-of-sight condition between the transmitter and the sensors over time.

Since there is no analytical expression for the probability density functions of the PRIDe test statistic, it was not possible to make a theoretical analysis of the detector's performance. The use of goodness-of-fit testes combined with artificial neural networks for the system-to-distribution parameter mapping problem, targeting numerically-computable expressions, is a promising semi-analytical solution to be investigated.

REFERENCES

- [1] L. Zhang, M. Xiao, G. Wu, M. Alam, Y. Liang, and S. Li, "A survey of advanced techniques for spectrum sharing in 5G networks," *IEEE Wirel. Commun.*, vol. 24, no. 5, pp. 44–51, Oct 2017.
- [2] Y. Arjoun and N. Kaabouch, "A comprehensive survey on spectrum sensing in cognitive radio networks: Recent advances, new challenges, and future research directions," *Sensors*, vol. 19, no. 1, 2019.
- [3] L. Chen, N. Zhao, Y. Chen, F. R. Yu, and G. Wei, "Over-the-air computation for cooperative wideband spectrum sensing and performance analysis," *IEEE Trans. Veh. Technol.*, vol. 67, no. 11, pp. 10603–10614, 2018.
- [4] The Institute of Electrical and Electronic Engineers, IEEE. (2011) IEEE 802 Part 22: Cognitive Wireless RAN Medium Access Control (MAC) and Physical Layer (PHY) Specifications: Policies and Procedures for Operation in the TV Bands.
- [5] D. Ramirez, G. Vazquez-Vilar, R. Lopez-Valcarce, J. Via, and I. Santamaria, "Detection of rank- p signals in cognitive radio networks with uncalibrated multiple antennas," *IEEE Trans. Signal Process.*, vol. 59, no. 8, pp. 3764–3774, Aug 2011.
- [6] L. Huang, Y. Xiao, H. C. So, and J. Fang, "Accurate performance analysis of Hadamard ratio test for robust spectrum sensing," *IEEE Trans. Wirel. Commun.*, vol. 14, no. 2, pp. 750–758, Feb 2015.
- [7] R. Zhang, T. J. Lim, Y. C. Liang, and Y. Zeng, "Multi-antenna based spectrum sensing for cognitive radios: A GLRT approach," *IEEE Trans. Commun.*, vol. 58, no. 1, pp. 84–88, Jan 2010.
- [8] L. Huang, H. So, and C. Qian, "Volume-based method for spectrum sensing," *Digital Signal Processing*, vol. 28, pp. 48–56, 2014.
- [9] L. Huang, C. Qian, Y. Xiao, and Q. T. Zhang, "Performance analysis of volume-based spectrum sensing for cognitive radio," *IEEE Trans. Wirel. Commun.*, vol. 14, no. 1, pp. 317–330, Jan 2015.
- [10] B. Nadler, F. Penna, and R. Garello, "Performance of eigenvalue-based signal detectors with known and unknown noise level," in *IEEE Int. Conf. Commun.*, Jun 2011, pp. 1–5.
- [11] D. A. Guimarães, "Gini index inspired robust detector for spectrum sensing over Ricean channels," *Electronics Letters*, vol. 55, no. 12, pp. 713–714, 2019.
- [12] S. Zhu, T. S. Ghazayy, S. M. R. Jones, R. A. Abd-Alhameed, J. M. Noras, T. Van Buren, J. Wilson, T. Suggett, and S. Marker, "Probability distribution of Rician K -factor in urban, suburban and rural areas using real-world captured data," *IEEE Trans. Antennas Propag.*, vol. 62, no. 7, pp. 3835–3839, Jul 2014.
- [13] B. V. Frosini, "Approximation and decomposition of Gini, Pietra-Ricci and Theil inequality measures," *Empirical Economics*, vol. 43, no. 1, pp. 175–197, Aug 2012.
- [14] M. Lin, W. Wang, X. Hong, and W. Zhang, "GLRT approach for multi-antenna based spectrum sensing under interference," *IEEE Commun. Lett.*, pp. 1–1, 2020.
- [15] D. A. Guimarães, "Pietra-Ricci index detector for centralized data fusion cooperative spectrum sensing," Jun 2020, doi: 10.24433/CO.456655.v5. [Online]. Available: <https://codeocean.com/capsule/4738960/tree/v5>.
- [16] A. L. Lemes, D. A. Guimarães, and Y. M. C. Masselli, "System-to-distribution parameter mapping for the Gini index detector test statistic via artificial neural networks," *Computers & Electrical Engineering*, vol. 85, p. 106692, 2020.
- [17] K. M. Captain and M. V. Joshi, "SNR wall for cooperative spectrum sensing using generalized energy detector," in *2018 10th Int. Conf. on Commun. Systems Networks (COMSNETS)*, 2018, pp. 143–150.
- [18] A. Bollig, C. Disch, M. Arts, and R. Mathar, "SNR walls in eigenvalue-based spectrum sensing," *EURASIP journal on wireless commun. and networking* : *EURASIP JWCN*, vol. 2017, no. 1, p. 109, 2017.